Published in final edited form as:
Pharm Res. 2014 June ; 31(6): 1460–1468. doi:10.1007/s11095-013-1102-8.

On-command drug release from nanochains inhibits growth of breast tumors

Pubudu M. Peiris[1,2,3], **Morgan Tam**[1,3], **Peter Vicente**[1,3], **Aaron Abramowski**[1,3], **Randall Toy**[1,3], **Lisa Bauer**[3,4], **Aaron Mayer**[1,3], **Jenna Pansky**[1,3], **Elizabeth Doolittle**[1,3], **Samantha Tucci**[1,3], **Erik Schmidt**[1,3], **Christopher Shoup**[1,3], **Swetha Rao**[1,3], **Kaitlyn Murray**[1,3], **Ramamurthy Gopalakrishnan**[2,3], **Ruth A. Keri**[5,6], **James P. Basilion**[1,2,3,6], **Mark A. Griswold**[2,3], and **Efstathios Karathanasis**[1,2,3,6,*]

[1]Department of Biomedical Engineering, Case Western Reserve University, Cleveland, Ohio

[2]Department of Radiology, Case Western Reserve University, Cleveland, Ohio

[3]Case Center for Imaging Research, Case Western Reserve University, Cleveland, Ohio

[4]Department of Physics, Case Western Reserve University, Cleveland, Ohio

[5]Department of Pharmacology, Case Western Reserve University, Cleveland, Ohio

[6]Case Comprehensive Cancer Center, Case Western Reserve University, Cleveland, Ohio

Abstract

Purpose—To evaluate the ability of radiofrequency (RF)-triggered drug release from a multicomponent chain-shaped nanoparticle to inhibit the growth of an aggressive breast tumor.

Methods—A two-step solid phase chemistry was employed to synthesize doxorubicin-loaded nanochains, which were composed of three iron oxide nanospheres and one doxorubicin-loaded liposome assembled in a 100-nm-long linear nanochain. The nanochains were tested in the Luc-GFP-4T1 orthotopic mouse model, which is a highly aggressive breast cancer model. The Luc-GFP-4T1 cell line stably expresses firefly luciferase, which allowed the non-invasive *in vivo* imaging of tumor response to the treatment using bioluminescence imaging (BLI).

Results—Longitudinal BLI imaging showed that a single nanochain treatment followed by application of RF resulted in an at least 100-fold lower BLI signal compared to the groups treated with nanochains (without RF) or free doxorubicin followed by RF. A statistically significant increase in survival time of the nanochain-treated animals followed by RF (64.3 days) was observed when compared to the nanochain-treated group without RF (35.7 days), free doxorubicin-treated group followed by RF (38.5 days), and the untreated group (30.5 days; n=5 animals per group).

Conclusions—These studies showed that the combination of RF and nanochains has the potential to effectively treat highly aggressive cancers and prolong survival.

[*]Author to whom correspondence should be addressed: Efstathios Karathanasis Wickenden Bldg. MS 7207, 10900 Euclid Ave, Cleveland, Ohio 44106, United States of America Phone: 216.844.5281; Fax: 216.844.4987; stathis@case.edu.

Keywords

Nanochain; multicomponent nanoparticle; triple-negative breast cancer; radiofrequency-triggered release; doxorubicin; chemotherapy; 4T1 cells; bioluminescence imaging

INTRODUCTION

While the enormous potential of nanoparticles for cancer drug delivery is universally accepted (1), current clinical practice indicates that nanoparticle-based chemotherapy does not show a consistently significant improvement in efficacy. While nanoparticles maximize the amount of drug in the tumor relative to normal tissues (1, 2), extravasated nanoparticles remain proximal to the vessel wall resulting in the drug being available primarily to cancer cells in the near-perivascular region of a tumor (3, 4). As shown in Fig. 1a, successful delivery to tumors requires that a long-circulating nanoparticle 1) enters the tumor microcirculation, 2) navigates through the tumor leaky vasculature into the tumor interstitium and 3) releases the drug to cytoplasmic targets of cancer cells. However, successful delivery of nanoparticles in tumors is limited by numerous biobarriers presented by tumors including low convective transport, high interstitial pressures, and large diffusion distances in the more avascular regions of a tumor. (3). In addition to the limited spread and penetration of nanoparticles due to these biobarriers, nanoparticles release their content slowly at the target site, which results in non-cytotoxic levels of the drug in the deep interstitium of tumors (5). While the slow release of content from nanoparticles does not favor cytotoxic effects, this is a required feature, since stable incorporation of the drug into the particle during blood circulation improves the drug's safety profile (6).

To improve the ability of a nanoparticle to spread its drug cargo throughout the tumor tissue, an elegant strategy is to liberate the content from nanoparticles after they extravasate into the tumor interstitium. Free drug in the tumor interstitium spreads widely within the tumor, and finally diffuses into subcellular compartments. In the case of doxorubicin (abbreviated as DOX), for example, nuclear DNA functions as a sink for the drug (5). In this context, we recently reported a multicomponent chain-shaped nanoparticle (7), which we termed nanochain. The nanochain is composed of three iron oxide (IO) nanospheres and one DOX-loaded liposome assembled in a 100-nm-long linear chain (Fig. 1b). In recent publications (7–9), we showed that the multicomponent nature and shape of the 100-nm-long nanochain resulted in a combination of three features leading to theranostic capabilities by simultaneously seeking, imaging and destroying tumors. Firstly, the nanochains exhibited enhanced deposition into tumors (7). Secondly, the chain-like shape (10, 11) and clustering of iron oxide cores (12, 13) substantially increased the T2 relaxivity per particle compared to their spherical counterparts, which allowed detection of low concentrations of the nanochains in tumors using MRI (8, 9). Thirdly, a mild radiofrequency (RF) field was able to trigger the release of DOX due to mechanical disruption of the liposomal membrane caused by the oscillation of the iron oxide "tail" of the nanochain (7). A detailed *in vitro* investigation of the mechanism of release showed that the response of nanochains to the applied 10 kHz RF field was mechanical oscillations (Fig. 1c) rather than local heating (7). Thus, contrary to heat-induced drug release, the nanochain's triggered release mechanism

was shown to be concentration-independent and based on mechanical forces that occur at the single particle scale. Using histological analysis, animal studies demonstrated that the RF-triggered release of DOX from nanochains resulted in a wide-spread cytotoxic effect throughout the entire tumor (7).

In this study, we examined the therapeutic outcome of the nanochain-based treatments using longitudinal imaging. We employed a neoadjuvant chemotherapy scenario, which uses chemotherapy in cases of localized primary tumors in order to decrease the size of the primary tumor before surgery. Neoadjuvant therapy is an increasingly attractive option in several scenarios for primary breast cancer therapy, especially in the cases of the aggressive breast cancer subtypes (*e.g.* triple-negative breast cancer) (14, 15). In addition to improved clinical outcome, a highly effective neoadjuvant therapy for locally advanced breast cancer has shown to result in improved breast preservation (14, 15). To test the nanochains in an animal model of triple-negative breast cancer, we used the 4T1 orthotopic animal model following orthotopic injection into the mammary fat pad of syngeneic, immune-competent mice. The 4T1 cell line is one of the few breast cancer models with a highly aggressive phenotype similar to that observed in the case of human triple-negative breast cancer (16, 17). Specifically, we used the Luc-GFP-4T1 cell line, which was engineered to stably express firefly luciferase (Luc) and green fluorescent protein (GFP) to allow *in vivo* using bioluminescence imaging (BLI) and non-invasive detection of cancer cells in histology using fluorescence microscopy. Thus, the progression of the disease could be measured using quantification of the BLI signal as a metric of therapeutic efficacy. Longitudinal BLI imaging demonstrated that a nanochain treatment in a neoadjuvant mode followed by application of an RF field significantly improved outcomes, inhibited the tumor growth of a highly aggressive breast cancer and decreased the overall tumor burden.

MATERIALS AND METHODS

Synthesis and characterization of nanochains

The nanochains were synthesized following our previously published method (7). Briefly, solid-phase chemistry was used to partially modify the surface functionality of nanospheres. CLEAR resin functionalized with amines was modified with a homobifunctional cleavable cross-linker reactive towards amines (DTSSP). Amine-functionalized IO nanospheres were introduced, allowed to bind to the solid support and then cleaved off using a reducing agent (TCEP). The same type of resin was used and the modified spheres with surface asymmetry were introduced in a step-by-step manner. As a final component, an amine functionalized DOX-loaded liposome was added before recovering the chain via a reducing agent. The chains were characterized in terms of their size (DLS), structure (TEM), and magnetic relaxivity (Bruker minispec relaxometer). To evaluate the effect of the geometry on the magnetization, we compared the r2 relaxivity of the nanochain particle to that of its parent IO nanospheres by measuring the transverse (R2) relaxation rates at 1.4 Tesla. Details of the synthesis and the analytical characterization of the DOX-NC nanoparticles are described in our previous publications (7, 9).

Mouse tumor model

All animal procedures were conducted under a protocol approved by the CWRU IACUC. We used an orthotopic 4T1 breast tumor model in mice (7, 8, 18). The Luc-GFP-4T1 cell line was engineered to stably express firefly luciferase and green fluorescent protein (GFP) to allow tracking and quantification of the cells in vivo and histologically. Briefly, we inoculated 0.5×10^6 4T1 cells orthotopically in a no. 9 mammary fat pad of female BALB/c mice that was surgically exposed while the mice were anesthetized. Starting 10 days after tumor inoculation, 200 μl of D-luciferin (10 mg/ml) were intraperitoneally administered and imaged after 10 min using a Caliper Life Sciences IVIS system. The animals were imaged every 2–3 days until the terminal point of the study. At the endpoint, organs were extracted and processed for histological analysis. The animals were used in the in vivo studies at week 2. We chose this time point, because it has been shown with BLI imaging and histology that this is the latest time point before the initiation of metastasis.

Survival study

Once the appropriate size of primary tumors was established with the Luc-GFP-4T1 tumor model (day 14), nanochain at a dose of 0.5 mg/kg DOX were IV injected via tail vein. After 18 hours from injection, animals were exposed to an RF field using a custom-made solenoid (N=105 turns, Inner Diameter=2.8 cm). The RF field (amplitude B=2 mT, frequency f=10 kHz, RF power=3–5 Watts) was applied for 60 min using the RF coil positioned 1 cm from the animal and oriented such that the magnetic field was directed toward the tumor. Following the same dose and schedule, groups included untreated animals (injected with saline), animals treated with free DOX followed by RF, and animals treated with nanochains without application of RF. The tumor growth was monitored using BLI imaging. The images were quantitatively analyzed using regions of interest (ROIs) that were manually drawn to measure luminescence in the primary tumor and “hot spots” in other organs (*i.e.* metastases). The signal in each hot spot was normalized to the background signal of the appropriate healthy organ. The time-course of the signal intensity of metastases in each animal included the summation of all the hot spots. The tumor growth was allowed to progress until the animals showed abnormal symptoms, at which point the animal were euthanized in a CO_2 chamber. Time of death was determined to be the following day.

Histological evaluation

To confirm the BLI images, *ex vivo* imaging and histological analysis of organs were performed on animals 30 days after tumor inoculation. Firstly, organs were explanted and imaged using a CRi Maestro fluorescence imaging system. Secondly, organs were histologically evaluated. Briefly, the animals were anesthetized with an IP injection of ketamine/xylazine and transcardially perfused with heparinized PBS followed by 4% paraformaldehyde in PBS. The primary tumors and organs were explanted and post-fixed overnight in 4% paraformaldehyde in PBS. The fixed tissues were soaked in 30% sucrose (w/v) in PBS at 4 °C for cryosectioning. Serial sections of 12 μm thickness were collected using a cryostat (Leica CM 300). The tissues were stained with the nuclear stain DAPI. Direct fluorescence of GFP (green) imaging of tumor and organ sections were performed for imaging the location of cancerous lesions. The tissue sections were imaged at 5× and 20× on

the Zeiss Axio Observer Z1 motorized FL inverted microscope. To obtain an image of the entire primary tumor or a large section of an organ (*e.g.* a liver or lung lobe), a montage of each section was made using the automated tiling function of the microscope.

Statistical analysis

Means were determined for each variable in this study and the resulting values from each experiment were subjected to one-way analysis of variance with post hoc Bonferroni test. A *P* value of less than 0.05 was used to confirm significant differences. Normality of each data set was confirmed using the Anderson-Darling test.

RESULTS

Nanochain synthesis

As shown in Fig. 2, the fabrication of nanochains is based on a two-step approach using solid-phase chemistry (7). In the first step, amine-functionalized IO nanospheres with a diameter of ~20 nm were attached on a solid support via a crosslinker containing a disulfide bridge. Liberation of the nanosphere using thiolytic cleavage created thiols on the portion of the particle's surface that interacted with the solid support resulting in a particle with two faces, one displaying only amines and the other only thiols. As a result, amines were converted to thiols with a topological control, generating a particle with asymmetric surface chemistry. Using solid-phase chemistry and step-by-step addition of particles, the two unique faces on the same IO nanosphere served as fittings to assemble them into linear nanochains. In the last step of synthesis, one DOX-loaded liposome was attached to the nanochain. Using a combination of extrusion and sonication, DOX-loaded liposomes were fabricated with a diameter of ~35 nm. This liposome size was comparable to that of the IO spheres. The final nanoparticle consisted of three IO spheres and one DOX-loaded liposome with the overall geometrical dimensions of the DOX-NC particle being about 100 × 30 nm (length × width), which was essentially the summation of the lengths of its constituent IO spheres and liposome. To evaluate the robustness of the nanochain synthesis, the nanochains were analyzed via visual inspection of multiple TEM images. The nanochains were synthesized in a highly controlled manner. Most of the nanochains are linear and consist of 4 members with the overall geometrical dimensions of the particle being about 100 × 20 nm (length × width). While <5% of the total particles in the suspension were the parent (unbound) IO spheres, the majority of the particles (83%) comprised of nanochains with three IO spheres and one liposome with the rest of the suspension being nanochains with 2 or 3 IO spheres. Due to the high intraliposomal space available for drug encapsulation and the efficient remote loading technique (19), the DOX cargo of DOX-NC was high (*i.e.* 6.8×10^{-5} ng/DOX-NC particle).

Therapeutic effectiveness in a mouse breast tumor model

Our goal was to evaluate the response of a primary tumor to the nanochain treatment in terms of growth rate of the tumor at the primary site and its subsequent metastatic spread to the rest of the body. Longitudinal BLI imaging of the untreated group of animals was performed every 2–3 days over a 7-week period after inoculation of the Luc-GFP-4T1 in a mammary fat pad. As shown in Fig. 3a, the growth of the primary tumor exhibited different

phases. After a rapid growth of the primary tumor during the first two weeks, the tumor growth plateaued for about 2 weeks followed by increased growth again in week 5. Metastasis became detectable by BLI for the first time in the thoracic region in the end of week 3. After that time point, metastatic growth increased rapidly. Figure 3b (y-axis is in logarithmic scale) shows the quantification of the BLI signal indicating that the development of metastases followed an almost exponential growth (inset shows the same graph with the y-axis being in linear scale). In addition to BLI imaging, histological analysis at day 14 after orthotopic tumor inoculation confirmed that cancer was only found at the primary site and had not yet spread elsewhere in the body. Thus, to replicate a therapeutic approach in a neoadjuvant mode, we treated the animals at day 14, because the tumor was restricted at its primary site, the mammary fat pad. Fig. 3c shows representative images of the group treated with a single injection of free DOX at day 14 followed by application of RF 18 h after injection. It should be noted that the administered dose was 0.5 mg DOX per kg of body weight. The tumor response was evaluated by quantitatively following the BLI signal over the period of weeks after treatment. In addition to the representative BLI images, quantification of the BLI signal (Fig. 3d) indicates that the DOX treatment resulted in negligible therapeutic benefits. BLI images of the group treated with a single application of the nanochain formulation (at day 14) are shown Fig. 3e. The nanochains were administered at a dose of 0.5 mg DOX per kg of body weight. While the treatment exhibited a moderate effect in the growth of the primary tumor, quantification of the BLI signal (Fig. 3f) indicates that metastatic spread was delayed by a few days compared to the untreated animals. However, the rate of metastatic spread quickly became similar to the untreated group.

On the other hand, the combination of nanochains and RF field resulted in a significant enhancement of the therapeutic outcome. The representative BLI images shown in Fig. 3g illustrate that a single treatment with nanochains at day 14 followed by the application of an RF field (18 h later), resulted in substantial shrinkage of the primary tumor and significant delay in the subsequent appearance of metastasis. More specifically, Fig. 3h quantitatively shows that the primary tumor started shrinking immediately after treatment as indicated by the 10-fold decrease of BLI signal between days 15 and 22. Most importantly, metastases appeared at a later time, which suggests the RF-triggered liberation of free DOX substantially delayed the growth of the primary tumor and its metastatic propensity in comparison to the other groups. To realize the degree of tumor response to the nanochain treatment followed by RF, Fig. 4 compares the four different conditions. As shown in Fig. 4a, the BLI signal in the primary tumor of animals treated with free DOX (with RF) or nanochains (without RF) was ~35-fold higher than that of animals treated with the nanochain treatment followed by RF. As a result of the RF-triggered release of DOX, the primary tumor shrank, which subsequently resulted in significant delay of the metastatic and aggressive behavior of the tumor. While the DOX treatment (with RF) or nanochain therapy (without RF) delayed the appearance of metastasis by 5 days compared to the untreated group (Fig. 4b), the growth rate of metastasis quickly became indistinguishable between these groups. However, the application of RF on nanochain-treated animals resulted in an outstanding 1000-fold lower BLI signal from metastases than the group treated with the nanochains (without RF) at their terminal point (~day 38).

To validate the BLI data and confirm the tumor presence in a qualitative manner, one animal (per condition) was euthanized at day 30 and organs were imaged *ex vivo* using a CRi Maestro fluorescence imaging system, since the Luc-GFP-4T1 cell line stably express GFP. Fig. 5a confirms the presence of widespread metastasis in the liver, spleen and lungs in the untreated and the nanochain-treated (without RF) animals. Grossly, the metastatic tumors appeared as white nodules in bright field imaging, compared to the darker liver parenchyma. Most importantly, the low fluorescence signal from organs in the animal treated with nanochains followed by RF indicates the presence of a very small number of cancer cells. Even though metastasis became apparent with BLI at day 26, the sensitivity of the method does not allow detection of the first few cancer cells that seeded the metastatic sites at an earlier time point (20, 21). Therefore, we histologically examined the same organs using fluorescence microscopy. Images of entire histological sections of the organs were obtained at a 5× magnification using the automated tiling function of the microscope. Representative images of liver and lung lobes are shown in Fig. 5b. While a large number of metastatic cancer cells (green) were found dispersed throughout the liver and lung tissues in the untreated and the nanochain-treated (without RF) animals, a very small number of clusters of metastatic cells were seen in the liver and lung parenchyma of the animal treated with nanochains followed by RF.

In addition, the therapeutic effect was determined by comparing the survival times of treated animals to untreated animals (Fig. 6). A statistically significant increase in survival time of the nanochain-treated animals followed by RF (64.3 ± 6.2 days; expressed as mean ± s.d.) was observed when compared to the free doxorubicin-treated group followed by RF (38.5 ± 2.5 days), the nanochain-treated group (35.7 ± 4.3 days) and the control group (30.5 ± 7.15 days).

DISCUSSION

In a recent publication (7), we introduced a new class of nanoparticles based on a multicomponent nanochain with an RF-triggered release mechanism that is based on mechanical vibrations occurring on a single nanochain particle. In those *in vivo* studies, we showed that DOX-loaded nanochains exhibited prolonged circulation and more effective extravasation into tumors than liposomes with diameters of 30 or 100 nm. However, both types of nanoparticles, nanochains and liposomes, exhibited the typical patchy, near-perivascular deposition in tumors. Furthermore, we histologically showed that the application of an RF field generated rapid and widespread release of free DOX throughout the entire tumor volume, resulting in substantial apoptosis of cancer cells throughout the entire tumor volume.

Here, we focused on evaluating the therapeutic efficacy of the nanochain treatment in the neoadjuvant mode in an animal model of triple-negative breast cancer. Among the subtypes of breast cancer (22), triple-negative breast cancer is an extremely aggressive and difficult-to-treat subtype. Even though triple-negative breast cancer represents 15–25% of invasive breast cancers, their aggressive and metastatic phenotype results in disproportional mortality among patients with breast cancer (23–25). In combination with surgery and radiation therapy, systemic chemotherapy, in its adjuvant and neoadjuvant modes, is the principal

treatment for triple-negative breast cancer. However, once metastases are developed, treating a metastatic lesion hidden within a large population of normal cells presents a unique challenge. It is clinically evident that combination of chemotherapy followed by surgical resection of primary tumor in metastasis-free patients typically results in successful therapeutic outcomes (26). Therefore, especially in the case of neoadjuvant chemotherapy, new agents are required to effectively reduce the growth of the primary tumor and prevent its spread before surgery, resulting in significant clinical impact (27, 28).

In this study, non-invasive BLI imaging was used to measure the response of triple-negative breast tumors. While caliper measurement of the size of a primary tumor provides a useful and quick metric, it cannot provide an exact measurement of the entire volume of the primary tumor. In addition, measurement of the primary tumor growth alone cannot inform us whether the disease has spread beyond the primary site. This information is very important especially in neoadjuvant scenarios, in which chemotherapy precedes surgical resection of primary tumor. More specifically, we non-invasively assessed the effectiveness of nanochain-based chemotherapeutic in terms of the spatiotemporal progression of breast cancer using longitudinal BLI imaging and the Luc-GFP-4T1 cell line. The orthotopic 4T1 mouse model is a mouse syngeneic and orthotopic mammary adenocarcinoma model displaying genetic compatibility of the tumor microenvironment with the host tissues in immune-competent animals (16, 17, 29–32). The aggressiveness and metastatic tendency of the animal model is directly related to the intact function of the immune system of the animal model. Previous studies have shown that growth of cells at the primary site displays a biphasic behavior (16): 1) the primary tumor rapidly grows in the first 2 weeks after inoculation of tumor cells in the mammary fat pad; 2) the tumor then shrinks over the next 2 weeks due to infiltration of leukocytes and extensive necrosis; 3) during the 4th week, the tumor grows again with metastases occurring primarily in the liver, spleen, and lungs. This is consistent with our observations as shown in Fig. 3a,b. Based on these findings, we elected to apply the nanochain and control treatments at day 14 after tumor inoculation, because the tumor was still confined at the primary site and had not yet invaded or metastasized.

Compared to the untreated animals, the growth of primary tumors treated with the DOX-loaded nanochain (without RF) was decreased, since nanochains exhibit selective deposition into primary tumors due to the Enhanced Permeation and Retention (EPR) effect. This is in good agreement with our previous publication (7), where we showed that the nanochains achieved a 2-fold higher deposition into primary tumors compared to 100-nm liposomes. Even with that enhanced deposition into tumors, the single application of the DOX-loaded nanochain treatment (without RF) provided only modest benefits. However, the application of RF on nanochain-treated animals significantly impacted the tumor progression. It should be emphasized that nanochain treatment was based on a low DOX dose (0.5 mg DOX per kg body weight). Typical dosage of liposomal DOX is 10–20 times higher and ranges from 5–10 mg/kg in preclinical and clinical studies (6, 33). Thus, since the RF pulse can be localized to organs of interest, the nanochain-based therapy has the potential of being highly effective using a low dose of chemotherapy.

CONCLUSION

In conclusion, we demonstrated that improvement of the temporal and spatial intratumoral distribution of chemotherapeutic drugs can achieve substantially improved outcomes as measured by BLI imaging. Considering the very low dose of the agent and that RF can penetrate deep into tissues, we envision that this platform technology could effectively deliver drugs to highly aggressive tumors with all the benefits of reduced side effects and substantial impact on cancer treatment.

Acknowledgments

We thank Kristen Lozada for help with the 4T1 tumor model. This work was partially supported by a grant from the American Cancer Society IRG-91-022-18 (EK) and a pilot grant from the Case Comprehensive Cancer Center P30 CA043703 (EK). L.B and R.T. were supported by a fellowship from the NIH Interdisciplinary Biomedical Imaging Training Program (5T32EB007509).

References

1. Ferrari M. Cancer nanotechnology: opportunities and challenges. Nat Rev Cancer. 2005; 5:161–171. [PubMed: 15738981]
2. Lasic DD. Doxorubicin in sterically stabilized liposomes. Nature. 1996; 380:561–562. [PubMed: 8606781]
3. Dreher MR, Liu W, Michelich CR, Dewhirst MW, Yuan F, Chilkoti A. Tumor vascular permeability, accumulation, and penetration of macromolecular drug carriers. Journal of the National Cancer Institute. 2006; 98:335–344. [PubMed: 16507830]
4. Yuan F. Transvascular drug delivery in solid tumors. Semin Radiat Oncol. 1998; 8:164–175. [PubMed: 9634493]
5. Laginha KM, Verwoert S, Charrois GJ, Allen TM. Determination of doxorubicin levels in whole tumor and tumor nuclei in murine breast cancer tumors. Clin Cancer Res. 2005; 11:6944–6949. [PubMed: 16203786]
6. Gabizon A, Goren D, Horowitz AT, Tzemach D, Lossos A, Siegal T. Long-circulating liposomes for drug delivery in cancer therapy: a review of biodistribution studies in tumor-bearing animals. Adv Drug Deliv Rev. 1997; 24:337–344.
7. Peiris PM, Bauer L, Toy R, Tran E, Pansky J, Doolittle E, Schmidt E, Hayden E, Mayer A, Keri RA, Griswold MA, Karathanasis E. Enhanced Delivery of Chemotherapy to Tumors Using a Multicomponent Nanochain with Radio-Frequency-Tunable Drug Release. ACS Nano. 2012; 6:4157–4168. [PubMed: 22486623]
8. Peiris PM, Toy R, Doolittle E, Pansky J, Abramowski A, Tam M, Vicente P, Tran E, Hayden E, Camann A, Mayer A, Erokwu BO, Berman Z, Wilson D, Baskaran H, Flask CA, Keri RA, Karathanasis E. Imaging metastasis using an integrin-targeting chain-shaped nanoparticle. ACS Nano. 2012; 6:8783–8795. [PubMed: 23005348]
9. Peiris PM, Schmidt E, Calabrese M, Karathanasis E. Assembly of linear nano-chains from iron oxide nanospheres with asymmetric surface chemistry. PLoS One. 2011; 6:e15927. [PubMed: 21253600]
10. Park JH, von Maltzahn G, Zhang LL, Schwartz MP, Ruoslahti E, Bhatia SN, Sailor MJ. Magnetic iron oxide nanoworms for tumor targeting and imaging. Advanced Materials. 2008; 20:1630–1635. [PubMed: 21687830]
11. Gossuin Y, Disch S, Vuong QL, Gillis P, Hermann RP, Park JH, Sailor MJ. NMR relaxation and magnetic properties of superparamagnetic nanoworms. Contrast Media & Molecular Imaging. 201010.1002/cmmi.387
12. Lu J, Ma S, Sun J, Xia C, Liu C, Wang Z, Zhao X, Gao F, Gong Q, Song B, Shuai X, Ai H, Gu Z. Manganese ferrite nanoparticle micellar nanocomposites as MRI contrast agent for liver imaging. Biomaterials. 2009; 30:2919–2928. [PubMed: 19230966]

13. Ai H, Flask C, Weinberg B, Shuai X, Pagel MD, Farrel D, Duerk J, Gao J. Magnetite-loaded polymeric micelles as ultrasensitive magnetic-resonance probes. Advanced Materials. 2005; 17:1949–1952.
14. Buzdar AU. Preoperative chemotherapy treatment of breast cancer--a review. Cancer. 2007; 110:2394–2407. [PubMed: 17941030]
15. Wolmark N, Wang J, Mamounas E, Bryant J, Fisher B. Preoperative chemotherapy in patients with operable breast cancer: nine-year results from National Surgical Adjuvant Breast and Bowel Project B-18. J Natl Cancer Inst Monogr. 2001:96–102. [PubMed: 11773300]
16. Tao K, Fang M, Alroy J, Sahagian GG. Imagable 4T1 model for the study of late stage breast cancer. BMC Cancer. 2008; 8:228. [PubMed: 18691423]
17. Dykxhoorn DM, Wu Y, Xie H, Yu F, Lal A, Petrocca F, Martinvalet D, Song E, Lim B, Lieberman J. miR-200 enhances mouse breast cancer cell colonization to form distant metastases. PLoS One. 2009; 4:e7181. [PubMed: 19787069]
18. Yori JL, Seachrist DD, Johnson E, Lozada KL, Abdul-Karim FW, Chodosh LA, Schiemann WP, Keri RA. Kruppel-like factor 4 inhibits tumorigenic progression and metastasis in a mouse model of breast cancer. Neoplasia. 2011; 13:601–610. [PubMed: 21750654]
19. Bolotin E, Cohen R, Bar L, Emanuel N, Ninio S, Lasic D, Barenholz Y. Ammonium sulfate gradients for efficient and stable remote loading of amphipathic weak bases into liposomes and ligandoliposomes. Journal of Liposome Research. 1994; 4:455–479.
20. Lelekakis M, Moseley JM, Martin TJ, Hards D, Williams E, Ho P, Lowen D, Javni J, Miller FR, Slavin J, Anderson RL. A novel orthotopic model of breast cancer metastasis to bone. Clin Exp Metastasis. 1999; 17:163–170. [PubMed: 10411109]
21. Aslaksonand CJ, Miller FR. Selective events in the metastatic process defined by analysis of the sequential dissemination of subpopulations of a mouse mammary tumor. Cancer Res. 1992; 52:1399–1405. [PubMed: 1540948]
22. Perou CM, Sorlie T, Eisen MB, van de Rijn M, Jeffrey SS, Rees CA, Pollack JR, Ross DT, Johnsen H, Akslen LA, Fluge O, Pergamenschikov A, Williams C, Zhu SX, Lonning PE, Borresen-Dale AL, Brown PO, Botstein D. Molecular portraits of human breast tumours. Nature. 2000; 406:747–752. [PubMed: 10963602]
23. Bertucci F, Finetti P, Birnbaum D. Basal breast cancer: a complex and deadly molecular subtype. Curr Mol Med. 2012; 12:96–110. [PubMed: 22082486]
24. Perreard L, Fan C, Quackenbush JF, Mullins M, Gauthier NP, Nelson E, Mone M, Hansen H, Buys SS, Rasmussen K, Orrico AR, Dreher D, Walters R, Parker J, Hu Z, He X, Palazzo JP, Olopade OI, Szabo A, Perou CM, Bernard PS. Classification and risk stratification of invasive breast carcinomas using a real-time quantitative RT-PCR assay. Breast Cancer Res. 2006; 8:R23. [PubMed: 16626501]
25. Bertucci F, Finetti P, Cervera N, Charafe-Jauffret E, Buttarelli M, Jacquemier J, Chaffanet M, Maraninchi D, Viens P, Birnbaum D. How different are luminal A and basal breast cancers? Int J Cancer. 2009; 124:1338–1348. [PubMed: 19058218]
26. Taketo MM. Reflections on the spread of metastasis to cancer prevention. Cancer prevention research. 2011; 4:324–328. [PubMed: 21372032]
27. Gao ZG, Tian L, Hu J, Park IS, Bae YH. Prevention of metastasis in a 4T1 murine breast cancer model by doxorubicin carried by folate conjugated pH sensitive polymeric micelles. J Control Release. 2011; 152:84–89. [PubMed: 21295088]
28. Wang Z, Yu Y, Dai W, Lu J, Cui J, Wu H, Yuan L, Zhang H, Wang X, Wang J, Zhang X, Zhang Q. The use of a tumor metastasis targeting peptide to deliver doxorubicin-containing liposomes to highly metastatic cancer. Biomaterials. 2012; 33:8451–8460. [PubMed: 22940213]
29. Pulaski BA, Ostrand-Rosenberg S. Mouse 4T1 breast tumor model. Curr Protoc Immunol. 2001; Chapter 20(Unit 20):22.
30. Gao ZG, Tian L, Hu J, Park IS, Bae YH. Prevention of metastasis in a 4T1 murine breast cancer model by doxorubicin carried by folate conjugated pH sensitive polymeric micelles. J Control Release. 152:84–89. [PubMed: 21295088]
31. Wendt MK, Molter J, Flask CA, Schiemann WP. In vivo dual substrate bioluminescent imaging. J Vis Exp.

32. Yori JL, Seachrist DD, Johnson E, Lozada KL, Abdul-Karim FW, Chodosh LA, Schiemann WP, Keri RA. Kruppel-like factor 4 inhibits tumorigenic progression and metastasis in a mouse model of breast cancer. Neoplasia. 13:601–610. [PubMed: 21750654]

33. Rose PG. Pegylated liposomal doxorubicin: optimizing the dosing schedule in ovarian cancer. Oncologist. 2005; 10:205–214. [PubMed: 15793224]

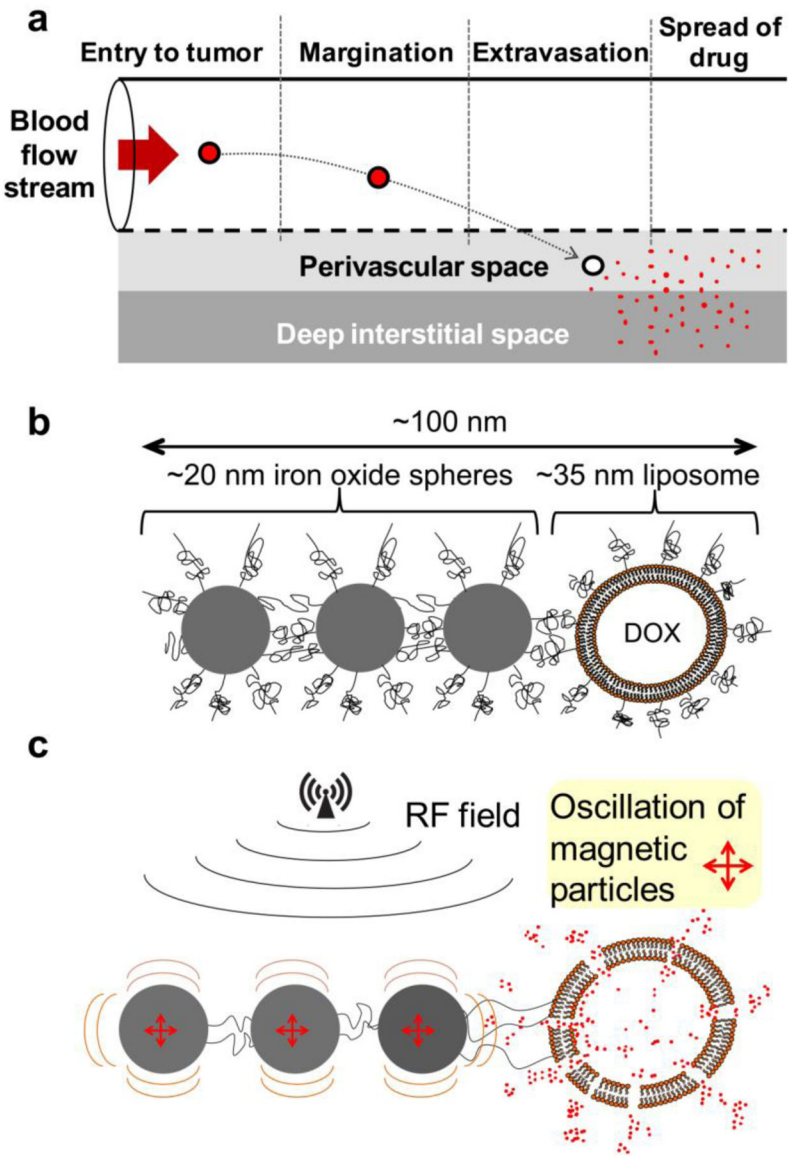

Figure 1.

(a) Illustration of the required steps for the successful delivery of nanoparticle-based drug to tumors. **(b)** A cartoon shows a linear nanochain composed of three IO nanospheres and one liposome. The constituent nanospheres display two distinctive faces in terms of chemical functionality, which allows them to be assembled into a linear nanochain. **(c)** The illustration of the triggered release mechanism shows that defects on the liposome are caused by the 'vibration' of the IO tail of the nanochain particle under an RF field.

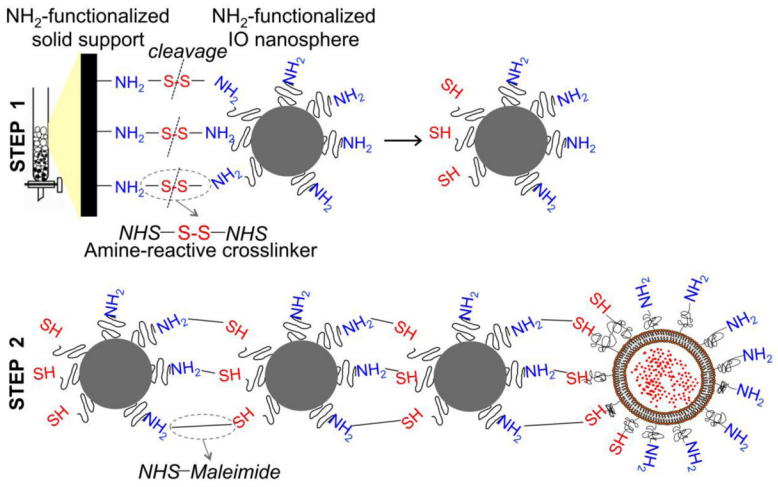

Figure 2.

Synthetic scheme of the partial modification of the functional groups on a nanospheres' surface (step 1) and the controlled assembly of linear nanochains (step 2).

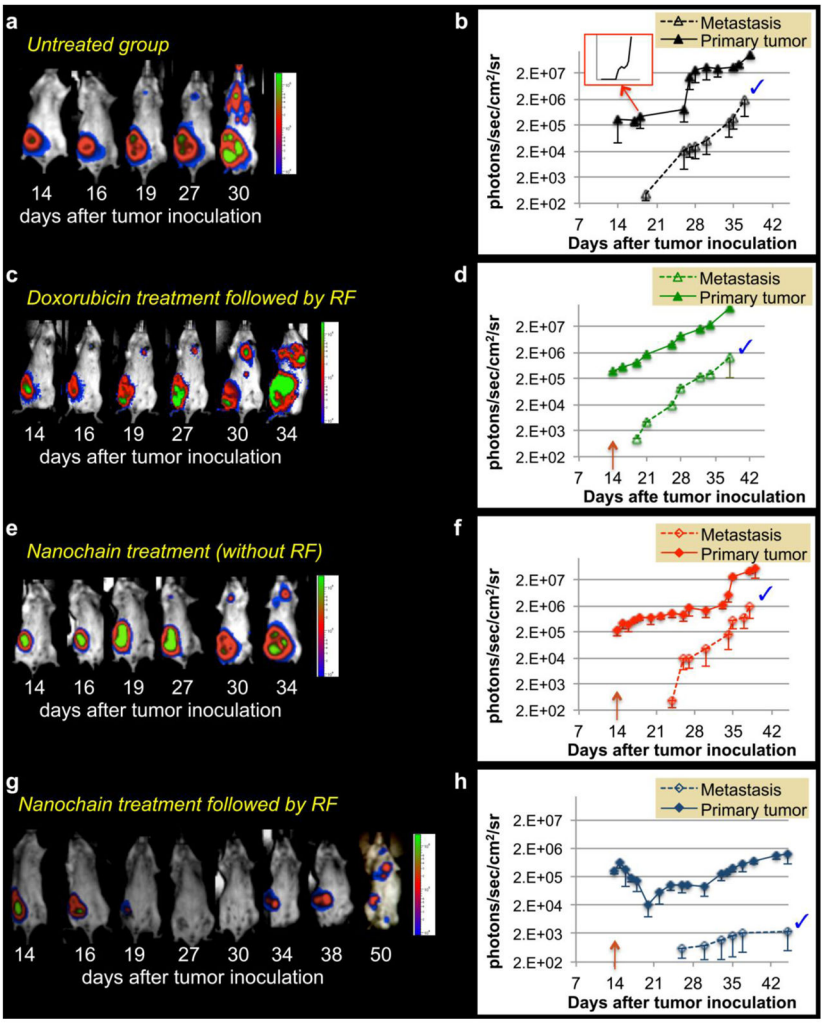

Figure 3.

Monitoring the progression of tumor growth and metastasis using BLI imaging. Luc-GFP-4T1 cells (0.5×10^{-6}) were implanted into the mammary fat pad of female BALB/c mice. Animals were imaged every 2–3 days over the period of 6 weeks. Besides an untreated group, animals were treated with DOX-loaded nanochains or free DOX (followed by RF) at a dose of 0.5 mg/kg DOX at day 14 after tumor inoculation. Representative images of longitudinal imaging are shown for **(a)** an untreated animal, **(c)** DOX-treated animal followed by application of an RF field 18 hours after injection **(e)** nanochain-treated animal, **(g)** and nanochain-treated animal followed by application of an RF field 18 hours after injection. Quantification of BLI light emission from primary and metastatic tumors over the six-week period is shown for **(b)** the untreated group (inset: the same plot is shown with the y-axis being in a standard linear scale), **(d)** the DOX-treated group followed by RF, **(f)** the nanochain-treated group, **(h)** and the nanochain-treated group followed by RF. Y-axis is in logarithmic scale. The blue tick mark indicates that all the data points between the two curves are statistically different ($P<0.005$; n=5 animals per group).

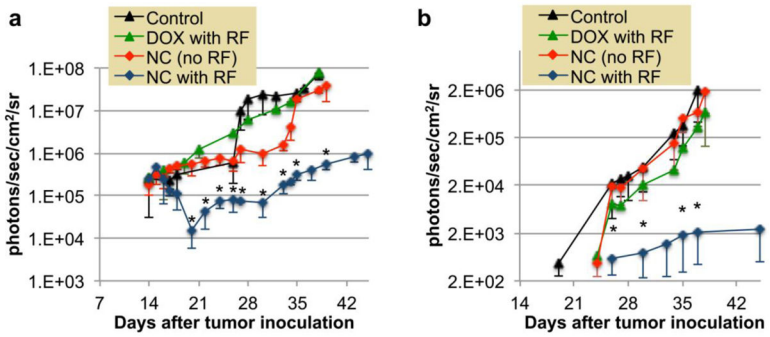

Figure 4.

Overall comparison of the BLI signal indicating the progression of **(a)** the primary and **(b)** metastatic spread of the untreated group (control), DOX-treated group (DOX with RF), the nanochain-treated group (NC-no RF), and the nanochain-treated group followed by RF (NC with RF). Y-axis is in logarithmic scale. Data points marked with asterisks are statistically different between the “NC with RF” group and the other groups. Data points marked with crosses are statistically different between the “NC(no RF)” group and the control group (* and † $P<0.05$; n=5–6 animals per group).

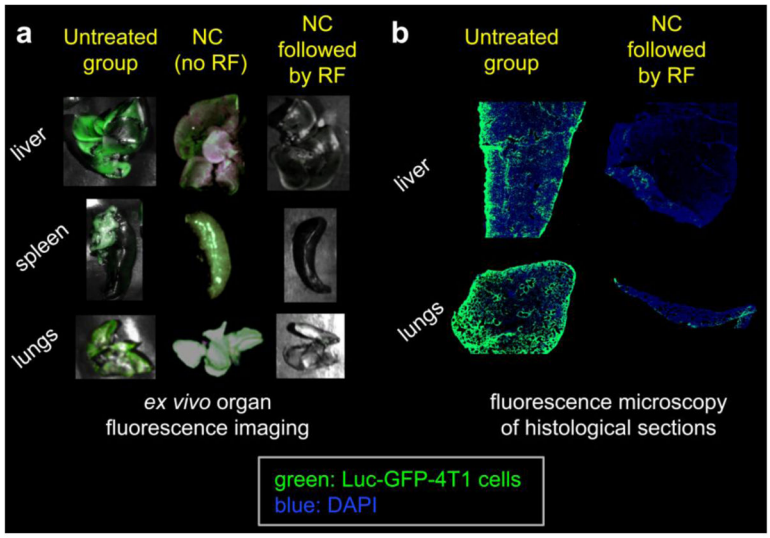

Figure 5.

(a) Evaluation of distribution of metastases using *ex vivo* imaging of organs. Organs from one animal per condition were excised 30 days after tumor inoculation and imaged using a CRi Maestro fluorescence imaging system. Green indicates the presence of Luc-GFP-4T1 cells. **(b)** Fluorescence images of entire histological sections of liver and lung lobes from the untreated animal and the nanochain-treated animal followed by RF (5x magnification; blue: nuclear stain (DAPI); green: Luc-GFP-4T1 cells). Images of entire histological sections of the organs were obtained using the automated tiling function of the microscope.

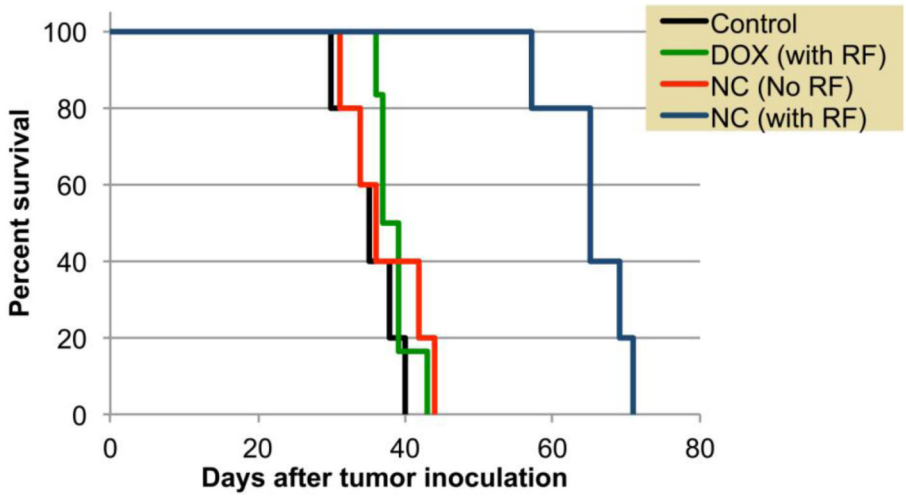

Figure 6.

The survival of the group treated with DOX-loaded nanochain followed by RF (n=5) was significantly prolonged when compared to the DOX-treated group followed by RF (n=6), the nanochain-treated group (n=5) and the untreated group (n=5).